Oriented Crosslinked Polyethylene Pipes by a Novel Extrusion Method

Jyri Järvenkylä[1], Bengt Johansson[2], Carl-Gustaf Ek[3], Magnus Palmlöf[3], Lisbeth Ahjopalo[4], Lauri Kuutti[4], Lars-Olof Pietilä[4], Bereket Neway[5], Ulf W. Gedde[5,*]

1. Uponor Group, P. O. Box 21, FIN-155 61 Nastola, Finland
2. Wirsbo Bruks AB, SE-730 61 Virsbo, Sweden
3. Borealis AB, SE-444 86 Stenungsund, Sweden
4. VTT Chemical Technology, P.O. Box 1401, FIN-02044 VTT, Finland
5. Royal Institute of Technology, SE-100 44 Stockholm, Sweden

* To whom all correspondence should be addressed.

SUMMARY: Crosslinking and stretching (2.5 times along the circumferential direction) of the molten polymer during extrusion produced pipes with dominantly circumferential orientation and a lower degree of axial chain orientation. Differential scanning calorimetry (crystallinity and crystal thickness), density measurements (crystallinity), X-ray diffraction (c-axis orientation), infrared dichroism measurements (crystalline and amorphous chain orientation) and contraction measurements (molecular draw ratio) assessed the microstructure of the pipe material. The mechanical properties of the oriented material were assessed by uniaxial tensile tests. The orientation was biaxial with the main orientation in the circumferential direction and a lesser orientation in the axial direction. The maximum degree of circumferential orientation was obtained at the inner wall of the pipe. The lower degree of crosslinking of the core material allowed slippage of chains during the stretching of the molten polymer and it is suggested that this is the cause of the lower degree of orientation of the core material. The oriented pipe material exhibited a 5-10% higher degree of crystallinity and higher crystal thickness than conventionally crosslinked material. The tensile modulus and the tensile strength of the oriented, cross-linked material was greater along the axial direction than along the circumferential direction. The circumferential and axial moduli for the oriented, crosslinked pipe were greater than the corresponding moduli of the non-oriented cross-linked pipe material. Another pipe based on crosslinked PE that were first circumferentially stretched 2.5 times and later axially stretched 10 times (in the molten state) showed, despite the fact that it exhibited pronounced axial orientation almost a balanced tensile modulus (4.3±0.2 GPa) in the axial-circumferential plane. Atomistic modelling showed that the orientational dependence of the density of the amorphous phase is small.

Introduction

During the past decades several attempts[1-5] have been made to produce plastic pipes with a circumferential molecular orientation to permit higher hoop stresses (internal pressures). Oriented PVC pipes, produced by expanding the extruded tube at a temperature (368 K) slightly above its glass temperature, have entered the market[5]. The presence of the tiny crystallites acting as physical crosslinks prevents slippage of the molecules past each other transferring the circumferential expansion effectively into circumferential orientation of the molecules.

 CCC 1022-1360/99/$ 17.50+.50/0

Several methods for have been proposed for orienting polyolefin pipes[1-4] but none of them has come into commercial use. The early efforts to produce oriented polymer pipes were concerned with hydrostatic extrusion[1,2]. Hope *et al.*[1,2] used a stationary mandrel and converging die arrangement which made possibly production of pipes at extrusion rates up to 20:1 but the extrusion rates were very low particularly at the higher extrusion ratios (a few mm per minute). These pipes showed remarkably good barrier properties and excellent resistance towards chemicals[6]. Later development by the Leeds group involved pulling the semi-crystalline polymer through a die without the application of any pressure (die-drawing), a process which allowed higher draw speeds[3,4]. PE and PP tubes with only axial and combined circumferential and axial orientation were made by die drawing at temperatures below the melting point (380-390 K for PE and 410-420 K for PP). PP pipes with a circumferential draw ratio between 2.3 and 3.3 showed a 50% increase in modulus and four-fold increase in tensile strength in the circumferential direction[4].

Orientation of polyethylene in the molten state can only be accomplished by first orienting the melt by extensional flow, i.e. by stretching the melt in the circumferential direction, followed by rapid stabilisation of the oriented structure by rapid cooling passed the crystallization temperature. Only thin-walled pipes can be cooled sufficiently rapidly to maintain the molecular orientation. Deformation of crosslinked polyethylene above its crystal melting point is a well-established technique for obtaining heat shrinkable products[7,8], including shrinkable pipes. In the patents to these products, there is no mentioning of molecular orientation being created by the expansion of the tubes above the crystal melting point. Samburski *et al.*[9] used a hot drawing process (408-418 K) to orient peroxide-crosslinked PE pipes. The drawn material showed an increase in melting temperature, degree of crystallinity and elastic modulus. The hot-drawn samples were characterised by the presence of a large amount of row nuclei with radiating lamellae showing a helical twist around the b-axis[9].

This paper presents a novel melt-extrusion method for creating circumferential chain orientation in pipes of crosslinked polyethylene. Tensile tests on specimens taken in different directions from the pipe wall indicated higher stiffness and strength than in pipes extruded without substantial stretching of the melt. A careful mapping of the microstructure through the pipe wall section of the oriented pipe was carried out by different experimental techniques providing data on molecular orientation and segmental orientation in the amorphous and crystalline components, degree of crystallinity, crystal thickness and crystal morphology. An additional pipe were made in the same extruder but the pipe were after the circumferential stretching stretched along the axial direction prior to the cooling past the crystallisation temperature region.

Experimental

Materials and preparation of pipes

A crosslinked and oriented PE pipe that was denoted PEXO with the dimensions 250x12 mm were produced by the novel extrusion method described in the next section. The melt was mainly stretched ($\lambda_C \approx 2.5$) along the circumferential direction. Another pipe (hereafter referred to as PEXO-A; dimension 250x1.2 mm) was prepared by the same method but after the circumferential stretching, the pipe was axially stretched approximately to $\lambda_A \approx 10$. These pipes were based on a linear polyethylene (Borealis, grade HE 2550) with $\overline{M}_n = 20\,000$ g/mol and $\overline{M}_w = 600\,000$ g/mol (size exclusion chromatography using linear PE standards and LALLS) containing a few percent of peroxide. The vinyl content was 0.6/1000 C by infrared spectroscopy and the room temperature density of the uncrosslinked material was 956 kg m^{-3}. Conventionally extruded crosslinked polyethylene pipes (hereafter referred to as PEX; dimensions -120x28 mm) based on the same base resin were made with the modified Engel method. Refs. 10 and 11 describe the original Engel method. A thermoplastic polyethylene pipe (denoted HDPE) was made in the same extruder using the same base resin containing no peroxide.

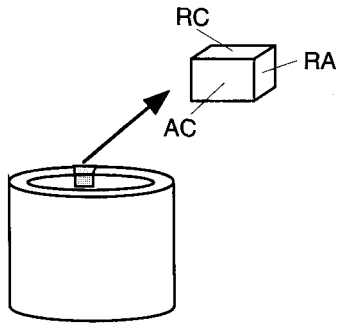

Fig. 1: Sampling from the pipe wall showing AC, RA and RC sample surfaces

Sampling from the pipes was in most cases obtained by sectioning parallel to the AC plane (Fig. 1). A few sections parallel to the RC and RA planes were also prepared.

Measurements

The tensile properties were obtained at 298 K in an Alwetron TCT10 tensile testing machine equipped with a digital extensometer. Bar shaped specimens, 6x1 mm cross- section and 50 mm effective length were used and the testing was carried out at two different cross-head speeds: 1 mm min^{-1} and 100 mm min^{-1}. A skiving machine was used to cut out the specimens from the pipe wall, both in the axial- and circumferential directions and in both cases at three

radial positions; at the inner- and outer wall and in the centre of the pipe wall. The stiffness, E-modulus, was measured as the maximum slope of the stress -strain curve. The stress recorded at 10% elongation was used as the measure of the material strength.

Bar-shaped specimens oriented both along the circumferential and axial directions were cut from different radial positions in the pipe wall. The specimens were pre-shrinked at 473 K. The lengths of the specimens after shrinkage were denoted L_0. The specimens were then subjected to a constant load (nominal stress $\sigma_n = 0.2$ MPa at 473 K and the lengths (L) of the specimens were measured after 20 min of load. By using the classical theory for rubber elasticity and assuming that the terminal chain segments do not contribute to the elastic force[12], the number average molar mass ($\overline{M}_c$) for the chain segments between the crosslinks was obtained from the following equation:

$$\sigma_n = \frac{\rho RT}{\overline{M}_c} \cdot \left(1 - \frac{2\overline{M}_c}{\overline{M}_n}\right) \cdot \left(\lambda - \frac{1}{\lambda^2}\right) \qquad \ldots(1)$$

where $\overline{M}_n$ is the number average molar mass of the polymer prior to crosslinking, R is the gas constant, T is the absolute temperature, ρ is the density of the material at 473 K (753.6 kgm^{-3}; Ref. 13) and λ is the draw ratio (L/L_0).

Micro-structural assessment was carried out on samples microtomed from the pipe wall at different depths. Mass crystallinity was obtained by differential scanning calorimetry (Mettler-Toledo 820) and by density measurements using a density gradient column (ISO 1872/2B-1183). The recorded heats of fusion (Δh_f) were converted into mass crystallinity (w_c) using the total enthalpy method[14] with 293 kJ (kg)$^{-1}$ as the heat of fusion ($\Delta h°_f$) for 100% crystalline polymer at 418.1 K, the equilibrium melting point[15] according to the expression:

$$w_c = \frac{\Delta h_f}{\Delta h_f^0 - \int_{T_1}^{T_m^0} \left(c_{p,a} - c_{p,c}\right) dT} \qquad \ldots(2)$$

where T_1 is an arbitrary temperature below the melting range, and $c_{p,a}$ and $c_{p,c}$ are the specific heats of the amorphous and crystalline phases, respectively. Data for $c_{p,a}$ and $c_{p,c}$ of Wunderlich and Baur[16] have been used. Mass crystallinity at 298 K was obtained from density data (ρ) according to:

$$w_c = \frac{\frac{1}{\rho} - \frac{1}{\rho_a}}{\frac{1}{\rho_c} - \frac{1}{\rho_a}} \qquad \ldots(3)$$

where ρ_c (=1000 kg m^{-3} [17]) and ρ_a (= 855 kg m^{-3} [17]) are the crystalline and amorphous densities at 298 K.

Crystalline chain orientation was assessed at 298 K by recording the X-ray diffraction pattern using a Statton camera using CuKα radiation or by using a Philips X'pert MPD in reflection mode using a counting detector. The azimuthal angle (ϕ; director was set parallel to the circumferential direction) of the (110) and (200) reflections (intensities are notified by I_{110} and I_{200}) were used to calculate the c-axis (001) orientation[18]:

$$\left\langle \cos^2 \phi_{110(200))} \right\rangle = \frac{\int_0^{\pi} I_{110(200)} \cos^2 \phi \sin \phi \; d\phi}{\int_0^{\pi} I_{110(200)} \sin \phi \; d\phi} \qquad \ldots(4)$$

$$f_{110(200)} = \frac{3\left\langle \cos^2 \phi_{110(200))} \right\rangle - 1}{2}$$

$$f_c = -f_{110} - f_{200} \qquad \ldots(5)$$

where f_c is the crystalline Hermans orientation function, f_{110} and f_{200} are the orientation functions of the (110) and (200) crystalline planes. It is important to note that most of the samples studied exhibited biaxial orientation and that the Hermans orientation function values quoted are only for comparative purposes since they are strictly only applicable to uniaxial orientation.

Infrared dichroism data were taken at 298 K on 20±2 μm thick microtomed samples using a Perkin-Elmer 1760 x FTIR instrument and a Bruker EQUINOX 55 FTIR instrument equipped with an Irscope II microscope. Each spectrum was based on 100 scans and polarized IR (parallel (p) and transverse (t) to the circumferential direction) was used to obtain the dichroic ratio ($R=A_p/A_t$; A is the absorbance). The Hermans orientation function (f_x) associated with the chain axis associated with absorption band (x) is given by[18]:

$$f_x = \frac{(R-1)\left(2\cot^2 \psi + 2\right)}{(R+2)\left(2\cot^2 \psi - 1\right)} \qquad \ldots(6)$$

where ψ is the angle between the transition moment vector and the chain axis.

The molecular draw ratio, i.e. the extension of the network junction points with respect to the non-oriented state, was obtained by heating microtomed samples above the melting point. The original dimensions of the samples were prior to heating as follows: circumferential (L_C^0): ~10 mm; axial (L_A^0): ~5 mm; radial (L_R^0): ~60 μm. The samples were for 2-4 min laid on a hot

stage (453±5 K) coated with silicone oil. The dimensions along cirumferential (L_C), axial (L_A) and radial (L_R) directions of the specimen were measured after cooling to 298 K. The molecular draw ratios in the three directions were obtained according to:

$$\lambda_C = \frac{L_C^0}{L_C};\ \lambda_A = \frac{L_A^0}{L_A};\ \lambda_R = \frac{L_R^0}{L_R} \qquad \ldots(7)$$

The average crystal thickness was obtained by DSC measurement of the melting peak temperature T_m, taking into consideration crystal thickening and superheating effects during heating according to Gedde and Jansson[19], using the Thompson-Gibbs equation[18]:

$$L_c = \frac{2\sigma_f T_m^0}{\Delta h_f^0 \rho_c \left(T_m^0 - T_m\right)} \qquad \ldots(8)$$

where σ_f=93 mJ/m^2 [15] is the surface free energy of the fold surface.

The lamellar structure of PEXO was revealed by atomic force microscopy (AFM, Scanning Probe Microscope Nanoscope III-a, Digital Instruments) after 18 h of etching at room temperature with a 1:1 mixture of sulphuric acid and phosphoric acid containing 0.7 wt.-% of $KMnO_4$ [20].

Atomistic simulation

The dependence of the density of amorphous oriented polyethylene on the degree of orientation has been studied by the Amorphous Cell method[21], originally developed by Theodorou and Suter[22], that was implemented in the MSI polymer modelling software. The amorphous structures were constructed by gradually adding bonds onto the polymer chains. The conformational states of the added bonds were predetermined by the conditional probabilities of the RIS theory[23] corrected by the increase in non-bonded interactions due to the added chain atoms and to the groups connected to them. In order to avoid artificial surface effects, periodic boundary conditions were used, *i.e.* when a chain leaves the periodic box its image comes into the box on the opposite side of the boundary. Identical replicas surround the central cell. Five cells having three chains with 200 carbon atoms were used. The initial amorphous structure was refined by repeated geometry optimisation carried out at constant temperature and pressure. The Compass force field implemented to the Polymer modelling software by MSI[21] was used in all the simulations. The cell edges of the optimised cells were about 2.5 nm.

The molecules were oriented by stretching the cell by gradually increasing a uniaxial stress. Disintegration of the cells was avoided by structural optimisation after each incremental increase

in stress. The density was calculated from the box volume and it was studied as a function of degree of orientation.

Description of Novel Process for Orienting XLPE Pipes

The extrusion method is based on the Engel method and is schematically described in Fig. 2. A more detailed description is presented in the patent literature[24]. The method differs from earlier methods in that the mechanical process that produces the circumferential orientation is carried out within the extrusion tooling. This arrangement provides many benefits: simplicity, possibilities to obtaining layered structures, inclusion of fibres and foams and controlled variation of degree of crosslinking. The molten polymer leaving the extruder can be drawn down before cooling below the crystal melting temperature range. Cooling was provided from both the inner and outer walls simultaneously.

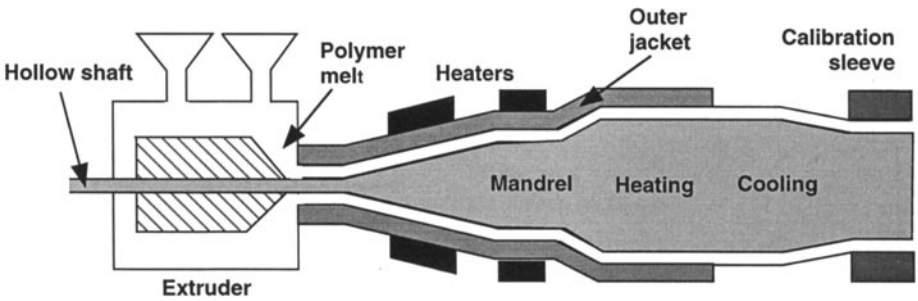

Fig. 2: Schematic illustration of the extrusion process

Melt extrusion was carried out at 473 K using an Engel extruder. The circumferential draw ratio (λ_C) defined by the ratio of the diameters before and after the melt stretch was 2.5. The pipe produced is referred to as PEXO. Another pipe, PEXO-A was prepared in the same extruder but in this case the pipe was in the final stage axially drawn down by $\lambda_A \approx 10$ prior to the cooling (solidification).

Results and Discussion

Mechanical data

The stress-strain data are displayed in Table 1. PEXO inner wall specimens showed higher tensile moduli and tensile strength, both axially (E_A) and circumferentially (E_C) than the specimens taken from the core and the outer wall. The tensile modulus was greater along the

axial direction than along the circumferential direction (*Table 1*). The strength of the inner wall specimens (PEXO) was the same for the axial and circumferential directions. The strength was however greater for the axial specimens than for the circumferential specimens at the core and the outer wall.

Table 1. Tensile testing data

Specimen code	Modulus-cirumferential (GPa) [a]	Modulus-axial (GPa)[a]	Strength (stress at 10% elongation) cirumferent/axial (MPa)[b]
PEXO			
Inner wall	0.96(0.47)	1.74(0.56)	29.7/29
Core	0.80(0.47)	1.40(0.73)	23.8/27.2
Outer wall	0.72(0.40)	1.42(0.53)	20.8/26.4
PEXO-A	4.1	4.1	26/96
PEX			
Inner wall	0.55 (0.32)	0.58 (0.31)	17.1/18.4
Core	0.71(0.47)	0.81(0.33)	22.4/22.3
Outer wall	0.75(0.27)	0.75(0.29)	18.6/18.4

a) Average value based on three tests. First value is from test performed at 100 mm/min; second value (within parenthesis) is from test performed at 1 mm min^{-1}. The values displayed were obtained from the maximum slope of the stress-strain curve.

b) Average value based on three tests.

The stiffness in the axial direction was ~ 100% larger for PEXO pipe than for PEX. The stiffness in the circumferential direction was considerably larger for PEXO than for PEX for the core and inner wall (75% greater) whereas the outer wall material showed a similar stiffness for PEXO and PEX. at the outer wall between PEXO and PEX. The strength values showed a 10 to 75% increase for PEXO pipe compared with PEX; the largest difference was obtained for the inner wall samples.

The stiffness data obtained, namely that $E_A > E_C$ may seem surprising, considering the findings presented in the next two sections that the chain orientation is mainly along the circumferential direction. However, Raumann and Saunders[25] showed for a series of oriented LDPE films stretched to different draw ratios (λ) between 1 and 5 that the room temperature

modulus along the draw direction showed a clear minimum at λ ~1.5. They also showed for specimens drawn to λ= 1-3 that the elastic modulus along the perpendicular direction in the film plane was greater than the modulus along the draw direction. The results can be explained on the basis of the aggregate model, which assumes that the material consists of anisotropic rods that rotate towards the draw direction. The draw ratio dependence of birefringence data obtained for LDPE and other materials was successfully described by the aggregate model[26]. Later Ward and co-workers[27-29] derived expressions for the compliance tensor as a function of degree of orientation and draw ratio. The following relationship holds for the elastic compliance (S'_{33}) along the draw direction:

$$S'_{33} = S_{11} \cdot \left\langle \sin^4 \theta \right\rangle + S_{33} \left\langle \cos^4 \theta \right\rangle + \left(2S_{13} + S_{44}\right) \left\langle \sin^2 \theta \cdot \cos^2 \theta \right\rangle \qquad \ldots(9)$$

where S_{ij} are the components of compliance tensor of the anisotropic aggregate, θ is the angle between the individual anisotropic rod and the draw direction. The reason for the appearance of a maximum in compliance at low draw ratios for LDPE at room temperature is that the third term in Eq. 9 becomes quite large because of the very high torsional compliance (S_{44}) of LDPE at room temperature[30]. Moderately stretched HDPE showed also a minimum (but less pronounced) in tensile modulus along the draw direction with increasing draw ratio[31]. The model also shows, as our experimental data indicates (Table 1), that the transverse elastic modulus is greater than the elastic modulus along the draw direction at low to moderate draw ratios.

PEXO-A showed, despite the fact that it exhibited pronounced axial orientation (Table 3), almost balanced stiffness properties in the AC plane (Table 1). This high stiffness in both axial and circumferential directions is truly remarkable and in accordance with earlier data presented for moderately stretched PE[25,31]. The pronounced difference in fracture stress obtained for axial and circumferential specimens was probably due to variations in surface roughness of the different samples.

Molecular draw ratio

Figure 3 shows the circumferential (C), axial (A) and radial (R) draw ratios of samples taken at different radial positions from the pipe wall of PEXO. The following relationship holds at all radial positions: $\lambda_C > \lambda_A > \lambda_R$. The product of the three draw ratios should, assuming constant volume, be equal to unity. The average of $\lambda_C \cdot \lambda_A \cdot \lambda_R$ was including all data points shown in *Figure 3* equal to 1.07. The highest draw ratios were recorded in the circumferential direction and thus the molecules were mainly oriented in this direction. However, the draw

ratios recorded for two other, perpendicular directions, were different (Fig. 3): the axial draw ratio was almost constant at unity through the cross-section, whereas the radial draw ratio was lower than one and exhibited a parabolic radial dependence. The draw ratio data thus indicate that orientation in the pipe wall is biaxial with the polymer molecules mainly oriented in the AC plane with considerably fewer chain segments oriented along the radius of the pipe. The circumferential draw ratio was highest near the inner wall, went through a minimum in the core and increased again towards the outer wall. The radial gradients of the draw ratios showed some positional dependencies, particularly near the inner wall. At some locations, there was a pronounced increase in the axial draw ratio approaching the inner wall, reaching values close to 1.5 at the inner wall. The inner wall values for the circumferential draw ratio were close to 2.5. Fig. 4 shows as a reference the draw ratios as a function of the distance from the inner wall for the supposedly non-oriented PEX pipe. Indeed, these samples showed only minor dimensional changes on heating.

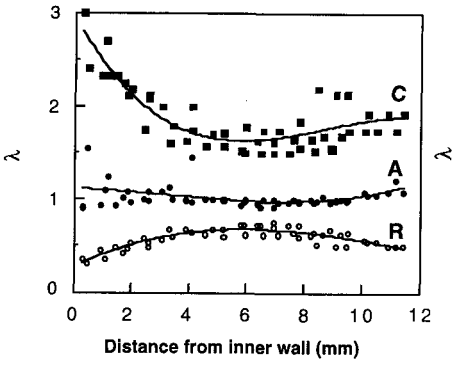

Fig. 3: Circumferential (C), axial (A) and radial (R) molecular draw ratios as a function of radial position of samples sectioned from PEXO

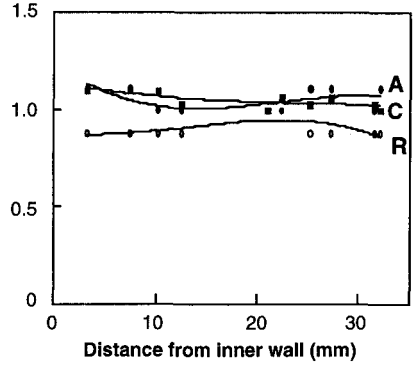

Fig. 4: Circumferential (C), axial (A) and radial (R) molecular draw ratios as functions of radial position of samples sectioned from PEX

An important question is how the obtained circumferential draw ratios compare with the draw ratio assuming maximum extension of the network chain segments. The average square end-to end distance ($\langle \bar{r}^2 \rangle$ for a polymer in the theta state is given by[23]:

$$\langle \bar{r}^2 \rangle = Cnl^2 \qquad ..(10)$$

where C is a constant depending of polymer and temperature which for PE at 410 K takes values near 7 [23], n is the number of main chain carbon atoms in a chain segment surrounded by two crosslinks and l is the carbon-carbon bond length which for polyethylene is 0.15 nm [23]. The maximum end-to-end distance (r_0) of the corresponding chain that it takes when it is fully stretched out is given by:

$$r_0 = \cos(30°)\ nl \qquad ..(11)$$

and the maximum draw ratio (λ_{max}) is the ratio between r_0 and r:

$$\lambda_{max} = \frac{r_0}{r} = \frac{0.866 \cdot \sqrt{n}}{2.6} \approx 0.33\sqrt{n} \qquad ..(12)$$

The number of carbon atoms in the chain segments between adjacent crosslinks should be in the range 300 to 600 (corresponding to molar masses of 4000 to 8000 g mol^{-1}) which result in λ_{max} values in the range 5.7 to 8.1. Thus, the highest circumferential draw ratio recorded for PEXO constituted 37% to 51% of the maximum attainable draw ratio.

Degree of crosslinking

The degree of crosslinking was assessed by measurements of the elastic modulus of the completely molten material and converting the elastic modulus data into the number average molar mass ($\overline{M}_c$) for the chain segments between the crosslinks by using Eq. 1.

Table 2. Degree of crosslinking of samples cut from PEX and PEXO

Radial position	$\overline{M}_c$(axial; g mol^{-1})	$\overline{M}_c$(circumfer.; g mol^{-1})
PEX-Inner wall	7300	8800
PEX-Outer wall	8200	5900
PEXO-Inner wall	8500	4000
PEXO-Core	Failure	13 400
PEXO-Outer wall	5800	5900

The data presented in Table 2 should only be considered as relative because the expression used to calculate $\overline{M}_c$ neglects the fact that a considerable part of the elastic stress is of enthalpic origin. It is clear that the degree of crosslinking of the core material is lower than that of the inner and outer wall materials (Table 2). The inner wall material showed anisotropic properties despite the fact that the specimens were given time to relax in the molten state prior to the mechanical loading. The elastic modulus was higher along the circumferential direction than

along the axial direction, hence the difference in the obtained $\overline{M}_c$ values (Table 2). It seems that the process, during its early development, did not provide sufficient heat to the core material to fully decompose the peroxide. The less densely crosslinked core material should show a greater tendency to relax after/during the circumferential stretching and hence to show a lower degree of circumferential orientation than the more tightly crosslinked inner-wall-material.

Crystallinity and crystal thickness

Data of crystallinity and crystal thickness obtained from density measurements and DSC are presented in Fig. 5. The crystallinities obtained from the two different methods were similar with a typical difference of 0.02. The degree of crystallinity was greater for PEXO than for PEX, with an average difference by ~0.05 (Fig. 5). The crystallinity was highest at the inner wall and it decreases with increasing distance from the inner wall for PEXO. This is unusual for pipes, which are cooled from both the inner and outer walls. In fact, both the non-oriented pipes showed the conventional crystallinity distribution with lower crystallinities for both the inner and outer wall samples (Fig. 5).

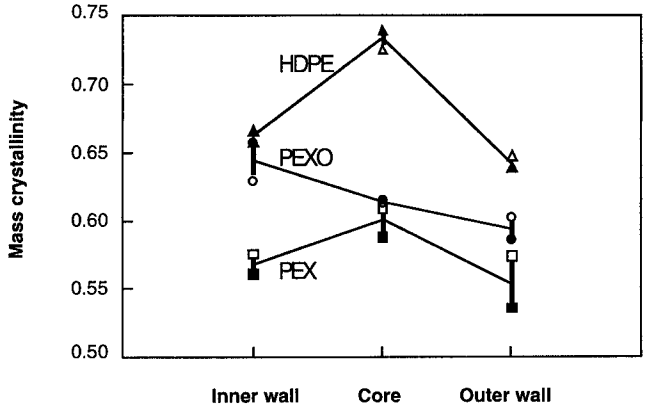

Fig. 5: Mass crystallinity by density and DSC at different radial positions in the pipe wall for PEX, PEXO and HDPE pipes

The reason for the very high degree of crystallinity at the inner wall sample of PEXO was the high circumferential orientation, which caused early (high temperature) crystallization[18]. There was a pronounced difference in melting peak temperature between PEXO and PEX - 4-8 K higher melting point for the PEXO samples-, which corresponds according to the Thompson-Gibbs equation to almost 10 nm thicker crystals in PEXO than in PEX (Fig. 6). The orientation of the molecules obtained in the extruder promotes early crystallisation and thus the formation of thicker crystallites[18].

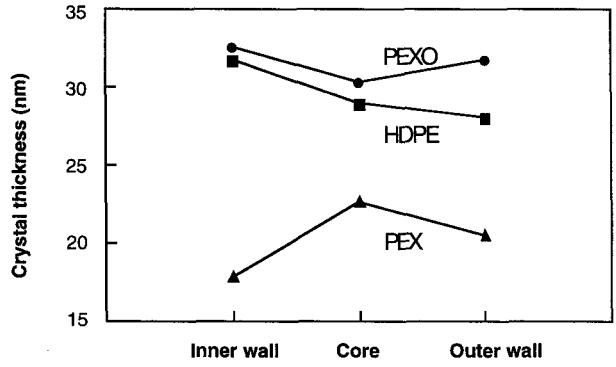

Fig. 6: Crystal thickness at different radial positions in the pipe wall for the different pipes studied

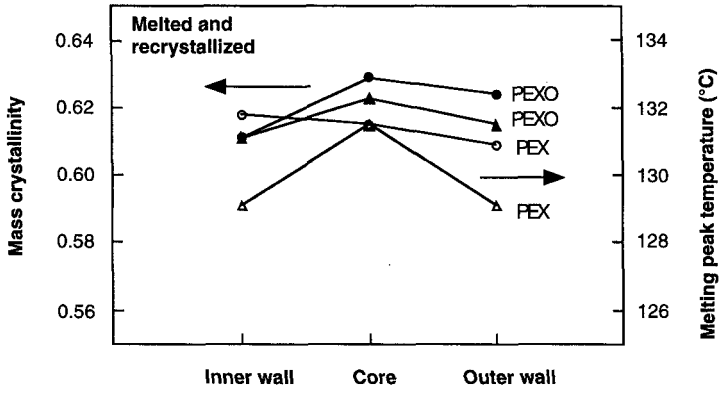

Fig. 7: Mass crystallinity and melting peak temperature at different radial positions in the pipe wall for melted and recrystallized samples

The samples were after the first melting (and shrinking) cooled at 10 K min^{-1} and then reheated while recording the melting thermogram. Most of the differences between PEXO and PEX in degree of crystallinity were absent after this heat treatment (cf. Figs. 6 and 7). The melting peak temperature was still somewhat lower for PEX than for PEXO, possibly indicating some difference in degree of crosslinking between the two materials.

The increase in degree of crystallinity and crystal thickness is very important for the stage I fracture behaviour. Data collected by Young[32] show that the yield stress is proportional to the degree of crystallinity at constant crystal thickness and it is also proportional to crystal thickness at constant degree of crystallinity.

Chain orientation

IR spectroscopy and WAXS assessed the chain orientation. It is important to note that most of the samples studied exhibited biaxial orientation and that the Hermans orientation function values quoted are only for comparative purposes since they are strictly only applicable to the case of uniaxial orientation. Figs. 8a and b show the polarised IR spectra of inner wall and mid section samples of PEXO, including both polarisation parallel and perpendicular to the circumferential direction (director).

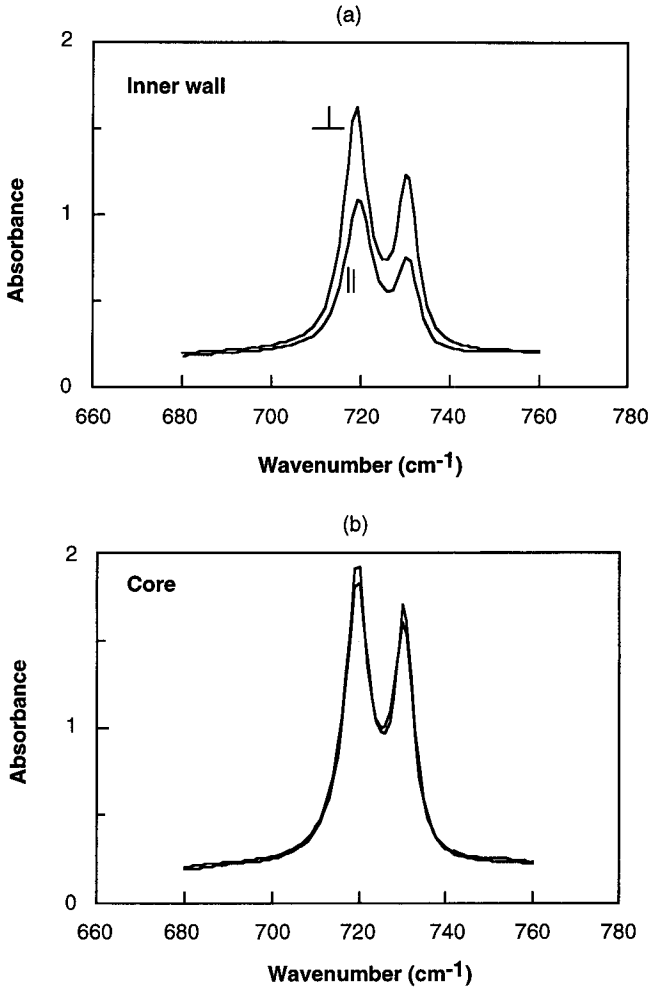

Fig. 8: IR spectra of samples cut along the AC plane from the inner wall (top) and the core (lower) of PEXO

Table 3. Degree of crystal orientation (f) in PEXO and PEXO-A

	Radial position-sample plane	f^a
PEXO:	Inner wall-AC plane	0.12, 0.20, 0.24, 0.24, 0.24, 0.29
	Core- AC plane	-0.06, -0.04, 0.02, 0.08, 0.10, 0.11, 0.11
	Outer wall- AC plane	0.04, 0.04, 0.06, 0.10, 0.12, 0.13
	Core- RC plane	0.04, 0.27, 0.28, 0.28
	Core- RA plane	0.12, 0.20, 0.23, 0.28
PEXO-A	Inner wall-AC	0.67
	Core- AC plane	0.50
	Outer wall-AC plane	0.83

a) The Hermans orientation function (assuming uniaxial symmetry). Director is for PEXO along the circumferential direction and for PEXO-A along the axial direction.

Figures 8a and b show the doublet CH_2 rocking vibrations. Both vibrations have transition moment vectors perpendicular to the chain axis[33]. The 730 cm^{-1} band is assigned to the crystalline component and it was used in the calculation of the Hermans orientation function. The two absorption peaks are overlapping and they were resolved by a mathematical procedure using two Lorentz functions. The almost indifferent spectra for the parallel and perpendicular polarised IR (vs. the director = circumferential direction) indicated that the c-axis orientation in the core is small whereas the pronounced dichroism found for the inner wall sample indicated crystal orientation in this sample. Table 3 shows the calculated f values obtained for the different PEXO samples.

The crystal orientation in the AC plane showed a pronounced radial dependence (Table 3). The orientation was mainly in the circumferential direction in the AC plane. The inner wall material showed the greatest degree of crystal orientation (f_c= 0.22±0.05) whereas the core showed only little crystal orientation (f_c= 0.05±0.07). The outer wall material was oriented (f_c= 0.10±0.05) to a lesser degree than the inner wall material. The shrinkage tests showed that orientation was mainly in the AC-plane and that the low f_c value obtained for the core is consistent with the relatively small difference between the circumferential and axial draw ratios (Fig. 3). The significant crystal orientation (f_c= 0.21±0.07) of the core material along the axial direction in the RA plane and along the circumferential direction (f_c= 0.21±0.11) in the RC plane further substantiates the biaxial character of the orientation in the pipe wall.

PEXO-A showed very pronounced axial orientation (note that the director is here defined as the axial direction). The outer wall exhibited the highest degree of orientation and, like for PEXO, the core exhibited the lowest degree of orientation (Table 3).

The amorphous orientation was calculated from the dichroism of two absorption bands. The 1078 cm^{-1} is associated with skeletal C-C stretching mode of both trans and gauche conformations in the amorphous phase[34]. The transition moment vector for this band is perpendicular to the chain axis[35]. The 1352 cm^{-1} has been assigned to the CH_2 wagging mode of amorphous chain segments[35] and the transition moment vector is perpendicular to the chain axis[33]. The dichroic ratios recorded for these bands were 1.05±0.05, also for the inner wall samples of PEXO. The amorphous orientation in the AC-plane was thus negligible in PEXO.

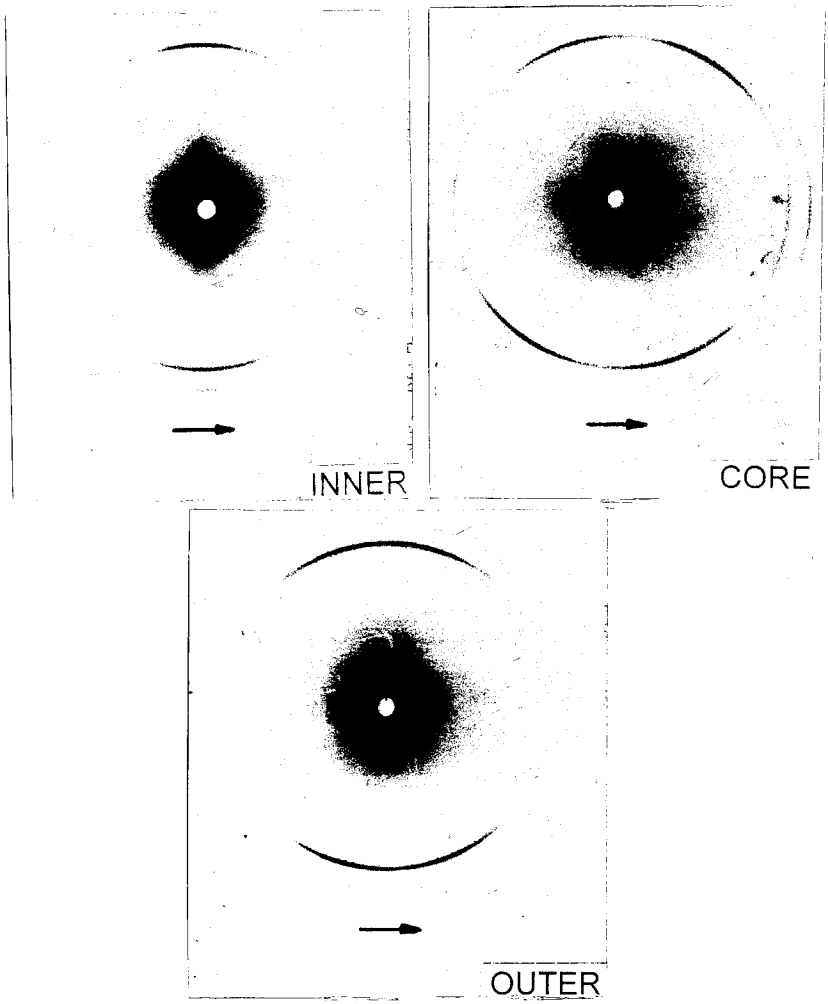

Figure 9. X-ray scattering patterns from PEXO samples (inner wall, core and outer wall). The incident X-ray beam was along the radius. The circumferential direction is indicated by arrows.

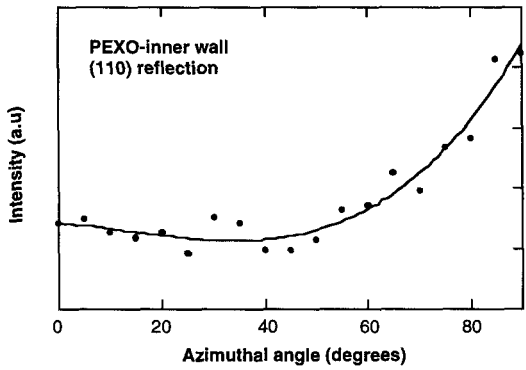

Fig. 10: Integrated intensity of the (110) reflection as a function of the azimuthal angle (0° is defined at the director which is along the circumferential direction).

Figure 10 displays the azimuthal angle dependence of the intensity of the (110) reflection for the PEXO-inner wall sample. The sample was cut along the AC plane, which is the plane, which is assessed by the displayed data. There is a biaxial character of the azimuthal angle dependence, a pronounced maximum at 90°, corresponding to the circumferential c-axis orientation, and a weaker maximum at 0° associated with the weaker axial orientation. The samples taken from the core and towards the outer wall showed basically the same kind of curves.

The Hermans orientation function was calculated assuming unixaial symmetry. It should be pointed out that this is not completely true but the data was calculated with the aim to compare the X-ray data with the corresponding data obtained by IR. The following f values were obtained for PEXO (data were based on both (110) and (200) reflections): 0.4 (inner wall); 0.3 (mid); 0.4 (outer wall). The c-axis orientations obtained from the IR data were lower, ranging from 0.2-0.3 for the inner wall to ~0 for the core. This seems at first sight very puzzling but it may be that the two methods sampled differently. It is proposed that the X-ray method underestimated the thinner crystals and that it primarily measured the c-axis orientation of the thicker crystals. Implicit in this statement is that the IR method more accurately measured the overall c-axis orientation. These data show, if this is true, that the first formed crystals had a very significant c-axis orientation whereas the crystals formed at the later states had a much lower degree of orientation. The crystals formed at the later stages are formed at lower temperatures that then cause their lower crystal thickness. Some relaxation must take place after the deformation period and hence it is natural the material that crystallise at a later stage also is less oriented.

X-ray diffractograms were also taken for samples cut along the RA plane thus assessing the orientation in this plane. The intensity of the (110) reflection showed only a weak azimuthal angle dependence for this particular sample.

Morphology

Figure 11 shows AFM micrographs of the inner wall of PEXO (AC plane). The permanganic acid etching has digested amorphous material and the crystal lamellae have dominantly perpendicular circumferential direction. Occasionally, crystal lamella stacks with different orientation were found.

The circumferential crystal chain orientation confirmed by X-ray scattering and IR spectroscopy is in accordance with the textures displayed by AFM: the lamellae normal, which is almost perpendicular to the chain axis is indeed mainly parallel to the cirumferential direction.

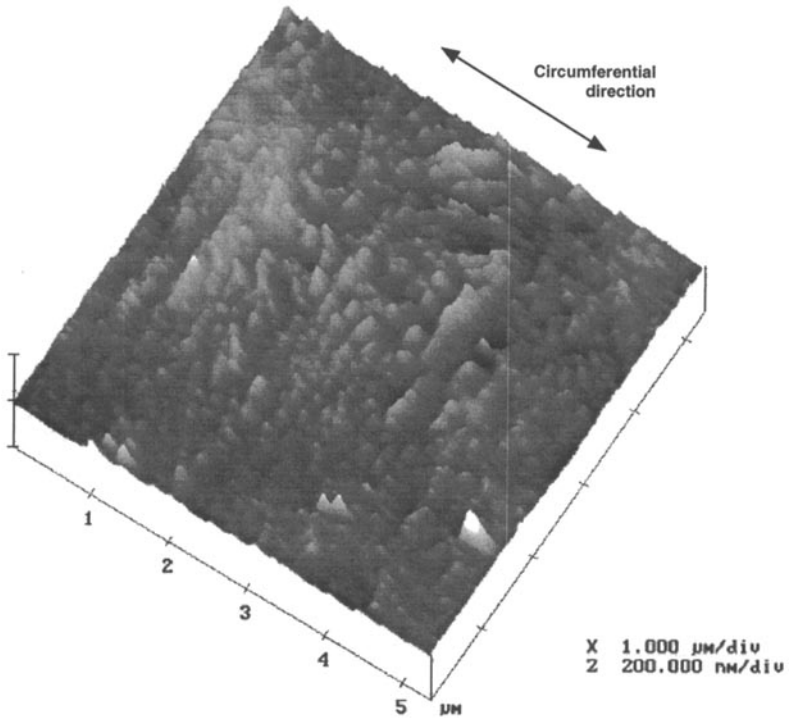

Fig. 11: Micrograph (AFM) showing the crystal lamellae texture (after etching with permanganic acid) on the AC plane from inner wall of PEXO. The circumferential direction is indicated with an arrow.

Amorphous density

The amorphous density was obtained from the atomistic modelling from the box volume and it was studied as a function of degree of orientation. The main interest was in the relative changes

of the density of the amorphous phase. It is important to consider possible changes in the amorphous density from ρ_a = 855 kg m^{-3} [17], obtained by extrapolating from data of the isotropic melt to room temperature.

Some examples of the structure of the simulated chains are displayed in Fig. 12. The density at 0 K of the isotropic cell was 912 kg m^{-3}. When the degree of orientation was small, with a cell edge length of 3-7 nm along the stress direction, the density of the optimised cells ranged between 855 – 880 kg m^{-3} with an average value of 866 kg m^{-3}. The proportion of the trans states increased from 0.56 in the isotropic cell to 0.62 – 0.70 in the stretched cells. Interchain movement thus dominantly accomplished the elongation of the cell. To conclude, remembering the approximate nature of Eq. 3, *i.e.* the extrapolation of the density of the amorphous phase and neglecting the crystalline-amorphous interphase, it is acceptable to use the constant value ρ_a = 855 kg m^{-3} in all pipe samples studied here.

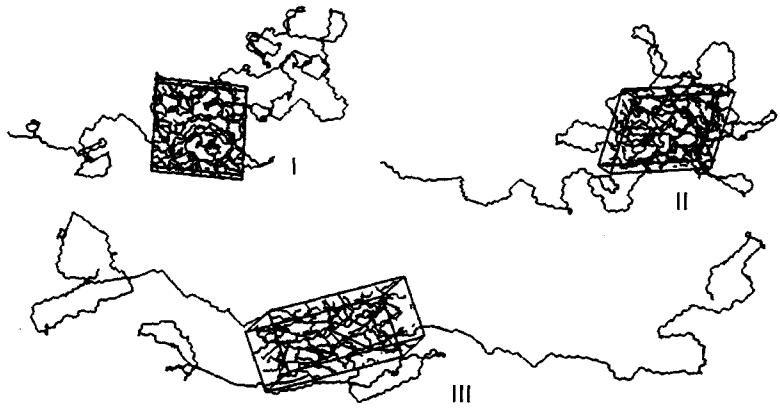

Fig. 12: Examples of amorphous structures in different stages of stretching: the parent chains are grey whereas the image chains in the central cell are black. For clarity, only the carbon atoms are shown. **I**: An unoriented cell. **II**: The cell at an early stage of stretching. **III**: The cell at a later stage of stretching, where one of the edges is ~ 6.9 nm.

Conclusions

Crosslinking and stretching of the molten polymer produced pipes with chain orientation. The orientation was biaxial with the main orientation in the circumferential direction and a lesser

orientation in the axial direction. The maximum degree of circumferential orientation was obtained at the inner wall of the pipe. The lower degree of crosslinking of the core material allowed slippage of chains during the stretching of the molten polymer and it is suggested that this is the cause of the lower degree of orientation of the core material. The oriented pipe material exhibited a 10% higher degree of crystallinity and higher crystal thickness than conventionally crosslinked polyethylene. The tensile modulus and the fracture stress of the oriented, crosslinked material was greater along the axial direction than along the circumferential direction despite the fact that the chain orientation is mainly along the circumferential direction. The stiffness and strength along the axial and circumferential directions were greater for the oriented, crosslinked pipe than for the corresponding pipe based on non-oriented crosslinked material. Another pipe based on crosslinked PE that were first circumferentially stretched 3 times and later axially stretched 10 times showed, despite the fact that it exhibited pronounced axial orientation almost balanced tensile modulus (4.3±0.2 GPa) in the axial-circumferential plane. Atomistic modelling showed that the orientational dependence of the density of the amorphous phase is small.

Acknowledgements

The reported has been sponsored by TEKES, Finland and by the International Science Program-the Asmara program, Uppsala (scholarship of Bereket Neway). The experimental assistance of T. Klasila and K. Kataja (VTT) is gratefully acknowledged.

References

1. P. S. Hope, A. G. Gibson, B. Parsons, I. M. Ward, *Polym. Eng. Sci.*, **20**, 540 (1980)
2. P. S. Hope S. Henderson, B. Parsons, I. M. Ward, *J. Mech. Working Tech.*, **5**, 223 (1981)
3. A. Selwood, I. M. Ward, B. Parson, *Plastic Rubber Process. Applications*, **8**, 49 (1987)
4. A. K. Taraiya, I. M. Ward, *Plastic Rubber Process. Applications*, **15**, 5 (1991)
5. M. J. Littlewood, in: *The Use of Plastics and Rubber in Water and Effluents*, PRI Conference, London (1982)
6. J. M. Marshall, P. S. Hope, I. M. Ward, *Polymer*, **23**, 142 (1982)
7. Patent DE 2719308
8. Patent US 3,201,503
9. G. Samburski, M. Narkis, A. Siegmann, *J. Mater. Sci. Lett.*, **15**, 1969 (1996)
10. T. Engel, Austrian Patent 309048 (1967)
11. T. Engel, *Kunststoffe*, **57**, 7 (1967)

12. P. J. Flory, in: *Principles of Polymer Chemistry*, Cornell University Press, Ithaca and London (1953)
13. H. Wilski, *Kunststoffe*, 54:10, 90 (1964)
14. A. P. Gray, *Thermochim. Acta*, 1970, 1, 563 (1970)
15. B. Wunderlich, in: *Macromolecular Physics*, Vol. 3, *Crystal Melting*, Academic Press, New York (1980)
16. B. Wunderlich, H. Baur, *Adv. Polym. Sci.*, 7, 151 (1970)
17. B. Wunderlich, in: *Macromolecular Physics*, Vol. 1, *Crystal Structure, Morphology, Defects*, Academic Press, New York (1973)
18. U. W. Gedde, *Polymer Physics*, Chapman & Hall, London (1995)
19. U. W. Gedde, J-F. Jansson, *Polymer*, **24**, 1521 (1983)
20. R. H. Olley, D. C. Bassett, *Polymer*, 1982, **23**, 1707 (1982)
21. *Polymer User Guide*, September 1996. San Diego: *Molecular Simulations* (1996)
22. D.N. Theodorou, U.W. Suter, *Macromolecules*, **18**, 1467 (1985)
23. P. J. Flory, *Statistical Mechanics of Chain Molecules*, Hanser, Munich, Vienna and New York (1989)
24. J. Järvenkylä, T. Josefsson, L. Ågren, B. Olsson, L. Hoving, M. Sjöberg, J. Rydberg, Y. Lundequist, *International Patent Application* W097/10941 (1997)
25. G. Raumann, D. W. Saunders, *Proc. Phys. Soc.*, **77**, 1028 (1961)
26. S. M. Crawford, H. Kolsky, Proc. Phys. Soc., **B64**, 119 (1951)
27. I. M. Ward, *Proc. Phys. Soc.*, **80**, 1176 (1962).
28. I. M. Ward, *Appl. Mater. Res.*, **5**, 224 and 258 (1966)
29. D. W. Hadley, P. R. Pinnock, I. M. Ward, *J. Mater. Sci.*, **4**, 152 (1969)
30. I. M. Ward, in: *Mechanical Properties of Solid Polymers*, 2nd Edition, Wiley, p. 282, (1985)
31. I. M. Ward, in: *Mechanical Properties of Solid Polymers*, 2nd Edition, Wiley, p. 280, (1985)
32. R. J. Young, *Materials Forum*, 210 (1988)
33. B. E. Read, R. S. Stein, *Macromolecules*, **1**, 116 (1968)
34. S. Krimm, *Fortschr. Hochpolym.-Forsch.*, **2**, 51 (1960)
35. J. R. Nielsen, R. F. Holland, *J. Mol. Spectrosc.*, **6**, 394 (1961)
36. R. G. Snyder, **47**, 1316 (1967)